Granular Matter (2016) 18:12
DOI 10.1007/s10035-016-0607-3

ORIGINAL PAPER

The influence of particle rolling and imperfections on the formation of shear bands in granular material

Hongxiang Tang[1] · **Yifeng Dong**[1] · **Xihua Chu**[2] · **Xing Zhang**[1]

Received: 31 October 2014 / Published online: 26 February 2016

Abstract This paper examines the development and evolution of shear bands in granular assemblies when particle rolling and imperfections are taken into account. Simulated biaxial tests in two-dimension are conducted using the discrete element method. The progressive development of rotational angles and effective strain are presented to describe the emergence and evolution of shear bands in biaxial tests. The simulated results reveal that when rolling resistance is taken into account in DEM, the development of shear bands is more distinct as the evolution of the minor shear bands is limited while the major shear bands are preferably promoted in granular materials, and that the local rotating bearings not only influence the onset of shear bands and the width of the shear bands, but also decrease the resistance and reduce the strength of the granular material. Also, it is demonstrated that the primary shear bands initiate from the imperfect areas and develop preferentially along the direction of imperfections. Therefore, the emergence and development of shear bands, which will result in a decline in strength and eventually lead to instability and destruction of the material, can be effectively simulated when rolling resistance is incorporated in DEM and the initial distribution of imperfections in the granular material is defined.

Keywords Rolling resistance · Imperfection · Shear band · Effective strain · Rotational angle

✉ Hongxiang Tang
tanghx@dlut.edu.cn

[1] State Key Laboratory of Coastal and Offshore Engineering, Dalian University of Technology, Dalian 116023, China

[2] Department of Engineering Mechanics, Wuhan University, Wuhan 430072, China

1 Introduction

Under an external load, the intense deformation of a granular material, such as dense sand, usually occurs in relatively concentrated narrow regions (called shear bands). This phenomenon is also called strain localisation and is usually related to the strain-softening property of the material. The mechanism for strain localisation and formation of shear bands is an important topic in the study of granular materials.

Granular materials are an assembly of discrete particles that are in contact at a microscopic level. It has been recognised that microstructure properties, such as particle packing, void ratios, and the evolution of void ratios, control the macroscopic behaviour of granular materials. The discrete element method (DEM) has been widely used to investigate the failure micro-mechanism of granular materials because of the ability to obtain the microscopic information at the particle level [1–6]. DEM allows for a contact model between two particles, viz. force-displacement law, for calculating the contact force. The physical properties and relative motion mechanism of particles in granular materials are reflected by contact models between particles. Using different contact models, different macroscopic behaviours can be achieved with DEM.

Oda et al. observed the microstructural changes and development of shear bands in a sand specimen using experiments combining an X-ray method with an optical method, which provided information about the thickness and direction of shear bands. Two conclusions have been drawn from these experimental results: there are great void ratios within the shear bands, and there are high rotational gradients of particles in the shear bands [7,8]. Also Bardet [9] observed the significant effects of particle rolling on the shear strength and consequently on the occurrence and evolution of shear bands

in particulate system. Through a two-dimensional granular Couette experiment, Veje et al. [10] revealed a separation of the kinematics into a slipping state and a nonslipping state consisting of a combination of rolling and translation. Astrom et al. [11] investigated a two-dimensional packing of elastic spheres, demonstrated that local "rotating bearings" are spontaneously formed in a shear band and that local rotating bearings play an important role in shear band formations. Alonso-Marroquin et al. [12] indicated that sliding and rolling are two outstanding deformation modes in granular media and that the introduction of rolling in the gouge dynamics could potentially explain the low friction of faults and low stress drops during earthquakes.

These phenomena can be replicated well only when rolling resistance is considered in DEM [13–15]. The importance of introducing the rolling resistance into the contact model has also been addressed by some researchers [16–18]. In most work, the rolling resistance moment at each contact is introduced as an additional component mechanism for taking into account the effects of particle rolling, but the rolling and the sliding friction tangential forces at contact, which should be constitutively related to the tangential components of the relative rolling and the relative sliding motion measurements respectively at the contact, are not distinguished. It should be noted that, as the relative motion that occurs at the contacting point is only or almost only the relative rolling, a model for tangential forces with omission of rolling friction tangential force may lead to unrealistic results in numerical calculations. Feng et al. [19] pointed out that correct modeling of rolling friction is still an under-developed area and many issues remain unanswered, and they developed a rolling resistance model and incorporated it within the sliding friction model. Li et al. [20] proposed a discrete element model, which can take into account both rolling resistances (rolling friction tangential force and rolling resistance moment) and sliding friction tangential force.

Void ratios and their distribution also play key roles in the macroscopic behaviour of granular materials [21,22]. Hermann argued that the distribution of void ratio is an important factor in the behaviour of granular materials [23]. In fact, local imperfections may relate with local uneven void ratio distributions in the granular specimen. The effects of initial imperfections on the initiation and development of shear bands in the sand specimen have been studied by some researchers using a macroscopic continuum [24]. For continuum, the information of shear bands can be described through macroscopic deformation, plastic strain and so on. While at the microscopic level of granular materials, it is not easy to get clear shear bands through describing the changes of particle positions or force chains or stresses or void ratios. From the previous work [7–9,13–18,20,25], the shear strain, volumetric strain, displacement vector and particle rotation are much better to show the information of shear bands occurred in granular materials.

Using DEM in two-dimension, this study will consider both rolling resistances (rolling friction tangential force and rolling resistance moment) and sliding friction tangential force between particles in the contact model, and attempt to investigate the effects of initial imperfections on the initiation and evolution of shear bands in granular materials. To easily understand and clearly describe the deformation process and the evolution of shear bands in granular materials, a macroscopic definition of effective strain for granular material is used. Besides, the rotational angles of the particles are displayed to describe the shear bands since there are high rotational gradients of particles in the shear bands from the experimental results [7,8]. In describing the progressive development of the effective strain and the rotational angles, the initiation and evolution of shear bands are simulated using different numerical tests considering free rolling, rolling resistance and no rolling for granular materials. Additionally, the effects of specimen imperfections on bearing capacity are analysed.

2 A contact model incorporating a particle rolling resistances mechanism

It should be noted that as the relative motion at the contacting point is mainly the relative rolling, a model for tangential forces with omission of rolling resistance may lead to unrealistic results in numerical calculations. Based on the work of Iwashatia and Oda [13,15], Li et al. [20], the contact model for calculation of tangential forces between two particles at contact, which incorporates both rolling resistances (rolling friction tangential force and rolling resistance moment) and sliding frictional force, is used here. This model is described in Fig. 1.

The normal contact force, the tangential contact force and the contact torque between particles A and B in contact are computed as

$$\begin{cases} f_n = k_n U_n + c_n \dfrac{dU_n}{dt} \\ f_t = f_s + f_r = \min\left(k_s U_s + c_s \dfrac{dU_s}{dt}, \mu_s |f_n|\right) \\ \qquad + \min\left(k_r U_r + c_r \dfrac{dU_r}{dt}, \mu_r |f_n|\right) \\ M_r = -\min\left(k_\theta \theta_r + c_\theta \dfrac{d\theta_r}{dt}, \mu_\theta r |f_n|\right) \end{cases} \tag{1}$$

where f_n is the normal contact force; f_t is the tangential contact force; f_s is the tangential sliding friction force; f_r is the tangential rolling friction force; M_r is the rolling friction

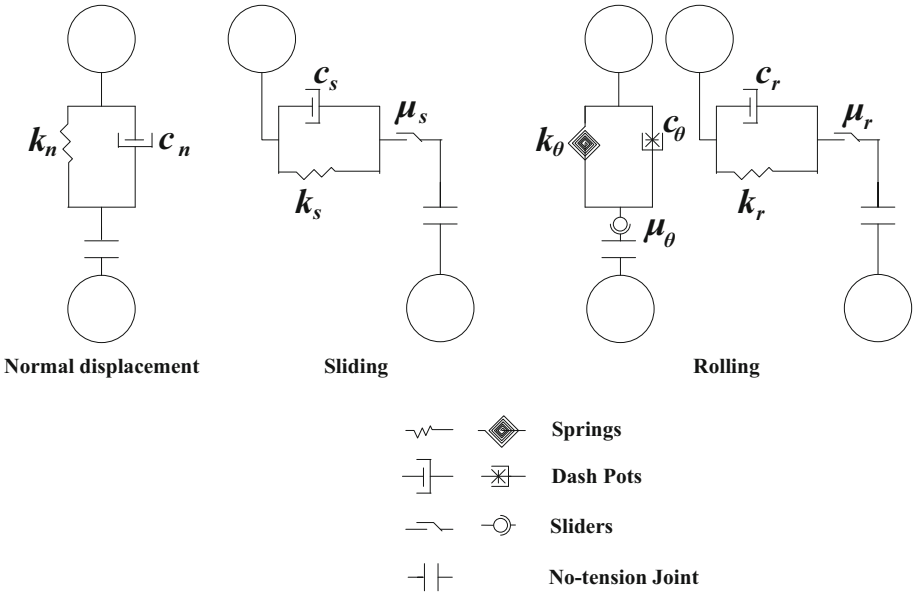

Fig. 1 The contact model incorporating both rolling resistances and sliding frictional force

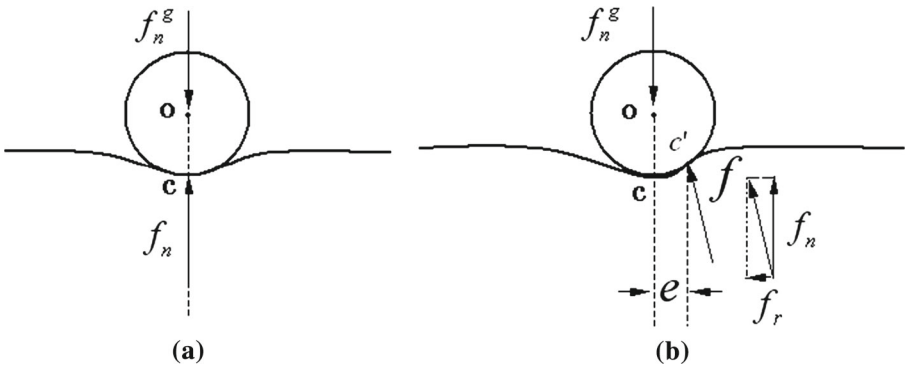

Fig. 2 The deformation of surface and supporting force (adapted from Chu [26]): **a** without rolling tendency; **b** with rolling tendency or being rolling

resistance moment; k_n is the stiffness coefficient of normal force; k_s is the stiffness coefficient of sliding force; k_r is the stiffness coefficient of rolling force; k_θ is the stiffness coefficient of rolling moment; U_n is the normal displacement; U_s is the tangential sliding displacement; U_r is the tangential rolling displacement; θ_r is the rolling angle; c_n is the viscous damping coefficient of normal force; c_s is the viscous damping coefficient of sliding force; c_r is the viscosity damping coefficient of rolling force; c_θ is the viscosity damping coefficient of rolling moment; μ_s is the sliding friction force coefficient; μ_r is the rolling friction force coefficient; and μ_θ is the rolling friction moment coefficient.

The rolling resistance considered here includes not only rolling moment, but also rolling friction force. The rolling friction force considered in the model is necessary for providing the energy dissipation under steady pure rolling state [19,20]. Up to rolling moment, when circular particle is used to model the real particle with irregular shape, the rolling moment is necessary for modeling accurately shear band of granular assemblies as the circular particle is easier to roll than irregular shape particle. Bardet, Iwashatia and Oda suggested similar rolling moment models and gave a relationship between rolling moment stiffness and slide stiffness [9,13,15]. Jiang et al. suggested the rolling moment stiffness is related to the normal stiffness, particle radius and the width of contact area [17]. From the mechanical and physical point of view, rolling moment and forces come from the bias of the resultant of contact normal force [26], as shown in Fig. 2, where f_n^g is the gravity of the particle.

3 Shear band failure of a perfect specimen

An 86.7 cm × 50 cm particle assembly specimen is considered. The specimen is generated with 4950 particles, each with an identical radius of 5 mm. Rigid plates, where compression forces will be applied, are set on the top and bottom of the specimen, as shown in Fig. 3. A pressure of 0.1 MPa is imposed around the specimen. The material parameters used in the analysis are presented in Table 1. In addition, the frictional coefficient between the rigid plates and the particles is 0.5.

To illustrate the effects of particle rolling resistance, four numerical biaxial compression tests (i.e., free rolling test, two

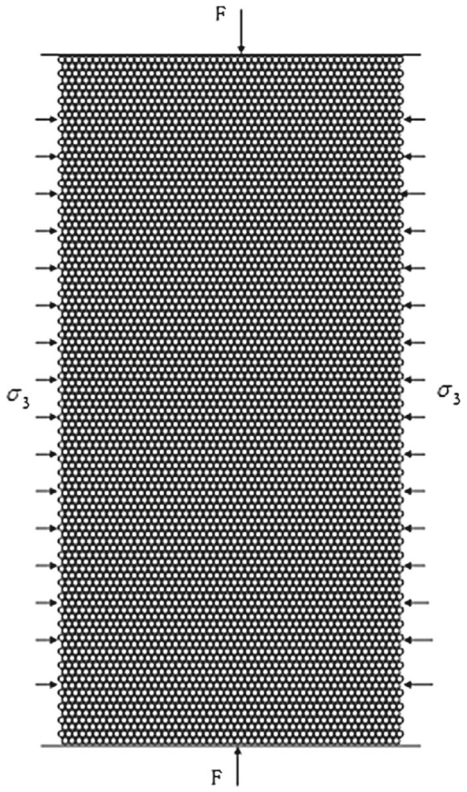

Fig. 3 A granular assembly of 4950 particles with radius of 5 mm collocates in a regular specimen

rolling resistance tests and no rolling test) are conducted. In each of the four tests, the loading and boundary conditions are the same, but different contact coefficients (i.e., different rolling stiffness, rolling moment stiffness, rolling damping, rolling moment damping, rolling friction and rolling friction moment coefficients) are adopted to reflect the free rolling, rolling resistance and no rolling mechanisms and presented in Table 2. During the compression process, the confining pressure is kept constant; the loading is applied continuously by displacement-control of the rigid plates, which are forced to move towards each other vertically. The numerical test results for each granular specimen, including the deformed configurations, effective strain distribution, particle rotational angles and axial stress-strain curves, are presented. The effective strain, which is defined at the centre of the particle to measure the change in position of a particle in relation to neighbouring particles, is briefly summarized in the "Appendix".

3.1 Free rolling

In this condition, no additional resistance against rolling is imposed on the rolling particles. Figure 4 shows the deformation of the specimen and the position of the particles at different axial strains. It can be seen that some large voids associated with large particle rotations (as can be seen in Fig. 6) appear in the middle of the final configuration. Figure 5 shows the effective strain distributions in the specimen for different axial strains indicating that a pair of wide shear bands develop gradually with the increasing axial strain in the specimen. The rotational angles of the particles relative to the initial position (clockwise rotation is positive, negative otherwise) for different axial strains are shown in Fig. 6, which illustrates a spontaneous formation of a local rotating ball bearing and high particle rotations in the wide and conjugate shear bands at the end of loading stage. However, they are distributed rather uniformly in both positive and negative sides. Astrom et al. [11] also stated that local "rotating bearings" are spontaneously formed in a shear band, and the bearings can be formed only when contacting grains rotate in different directions, and therefore there is a concentration of both clockwise and counterclockwise rotations in the shear bands. The similar observations were reported by Oda et al. [7,8,25].

The deviatoric stress-axial strain curve for the specimen in the free rolling test, shown in Fig. 7, illustrates that peak

Table 1 Parameters for DEM simulation

Parameters	Particle density (kg/m^3)	Normal spring constant (N/m)	Tangential spring constant (N/m)	Normal damping constant (N)	Tangential damping constant (N)	Slide friction coefficient
Value	2600	2.5×10^8	2.0×10^8	0.02	0.02	0.5

Table 2 Contact coefficients for different tests

	Rolling stiffness (N/m)	Rolling moment stiffness (Nm/rad)	Rolling damping (Ns/m)	Rolling moment damping (Nms/rad)	Rolling friction	Rolling friction moment
Free rolling	0	0	0	0	0	0
Rolling resistance 1	1.0×10^6	2.5	0.1	0.1	0.1	0.1
Rolling resistance 2	1.0×10^7	2.5	0.7	0.7	0.7	0.7
No rolling	1.0×10^8	2.5	1.0	1.0	1.0	1.0

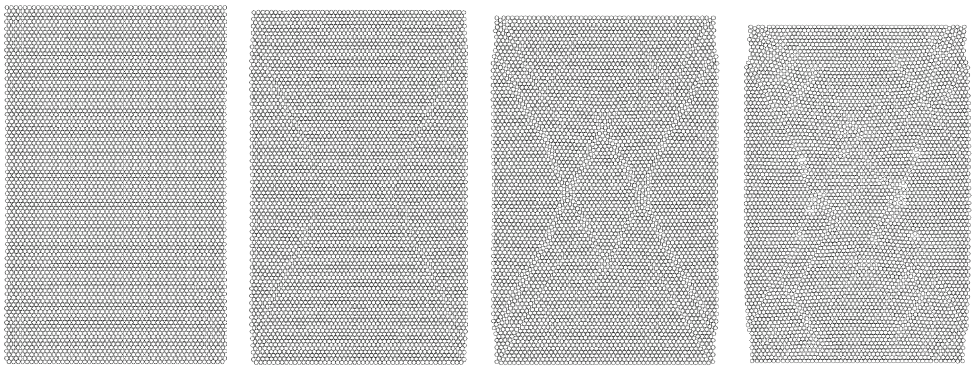

Fig. 4 The positions of the particles at different axial strains in the sample

(a) 0.7% **(b)** 2.1% **(c)** 3.5% **(d)** 4.9%

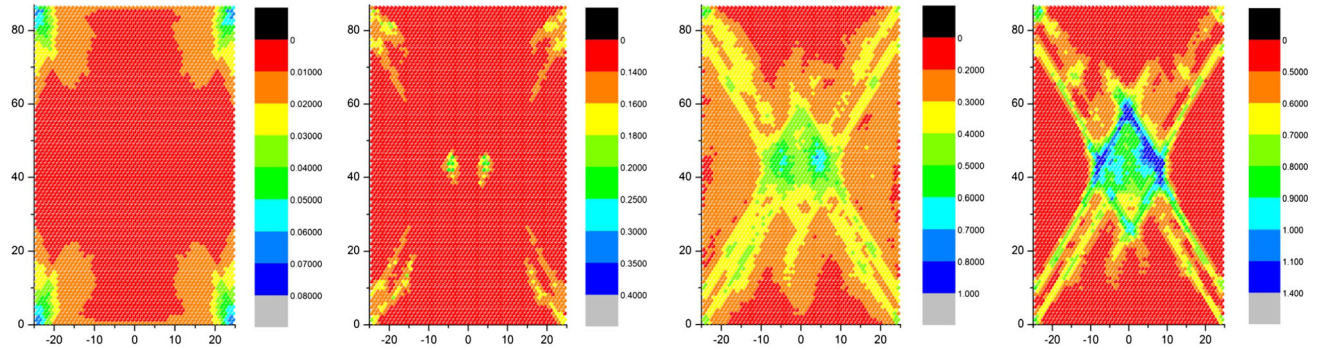

(a) 0.7% **(b)** 2.1% **(c)** 3.5% **(d)** 4.9%

Fig. 5 The effective strain distributions in the specimen with increasing axial strain in free rolling test

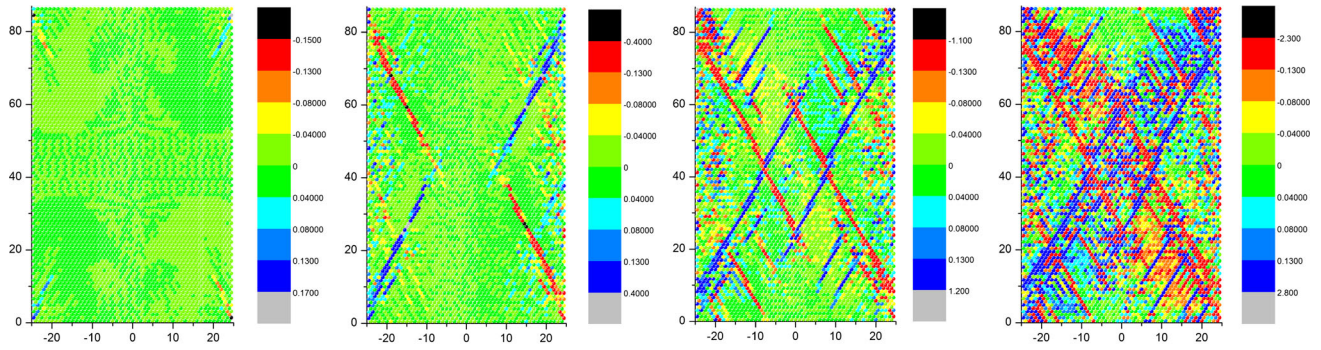

(a) 0.7% **(b)** 2.1% **(c)** 3.5% **(d)** 4.9%

Fig. 6 The rotational angles distributions in the specimen with increasing axial strain in free rolling test

strength arrives at 2.1 % axial strain and then declines gradually until a residual value arrives at 5 % axial strain. From Figs. 5 and 6, it can be seen that the shear bands initiate around the peak strength and develop to concentrate in one pair of wide and conjugate shear bands afterwards.

3.2 Rolling resistance 1 and 2

In these conditions, the particles are not allowed to roll until the rolling torques acting on the particles are greater than a threshold value. The results are similar to the case of free rolling. Two conjugate shear bands can be seen along the diagonal lines in the final configuration. Figure 8 shows the effective strain distributions in the specimen for different axial strains indicating that a pair of persistent and distinct shear bands develop gradually with the increasing axial strain.

The rotational angles of the particles relative to the initial position for different axial strains are shown in Fig. 9, which illustrates that compared with Fig. 6, some lower particle rotations appear in narrower zone in the specimen at the end of loading stage.

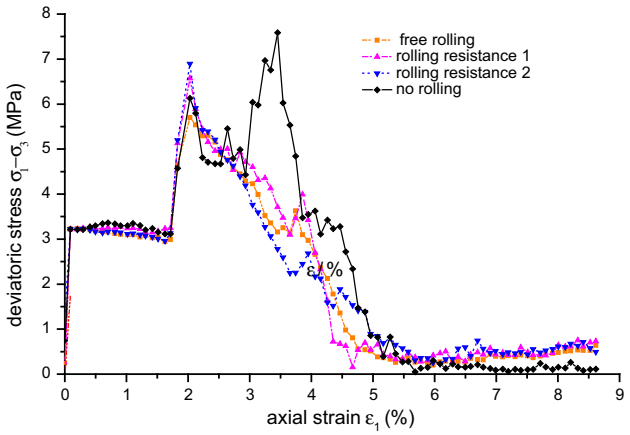

Fig. 7 The deviatoric stress-axial strain curves for the granular assembly in biaxial test of a perfect specimen

Compared with the free rolling test, it can be observed that only two major and conjugate shear bands are promoted, and the width of shear bands are narrower in this test. It demonstrated that local rotating bearings play an important role in shear band formations and influence both the onset of shear banding and the width of the shear bands.

3.3 No rolling test

In this condition, particle rolling is prevented, and particle sliding is the primary movement pattern.

Figure 10 shows the effective strain distributions in the specimen at different axial strains, indicating that no regular shear bands are developed in the specimen. The rotational angles of the particles relative to the initial position for different axial strains are shown in Fig. 11, illustrating that some extremely low particle rotations randomly distribute in the sample.

The deviatoric stress-axial strain curve for the specimen in this condition, shown in Fig. 7, illustrates that peak strength is distinctly higher than that in previous three tests, and arrives at a delayed axial strain of 3.5 % because the particles can not move smoothly due to rolling restriction. It indicates that particle rolling may decrease the resistance and reduce the strength of the granular material.

Alonso-Marroquín et al. [12] indicated that the deformation of the granular material is dominated by rigid-body motion due to the vorticities, rolling due to the rotational bearings and elastic dislocation due to building of force chains, and that spontaneous formation of vorticity cells assisted by

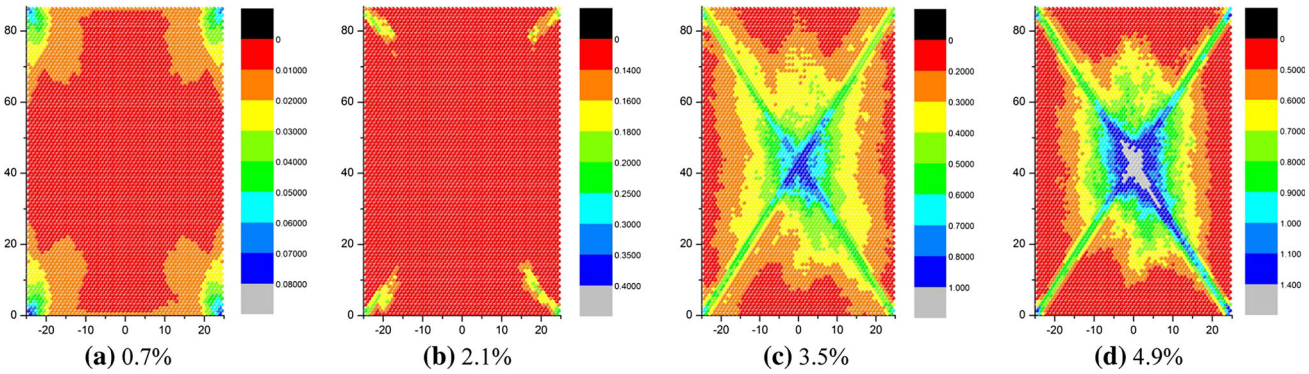

Fig. 8 The effective strain distributions in the granular assembly withincreasing axial strain of the assembly in rolling resistance test

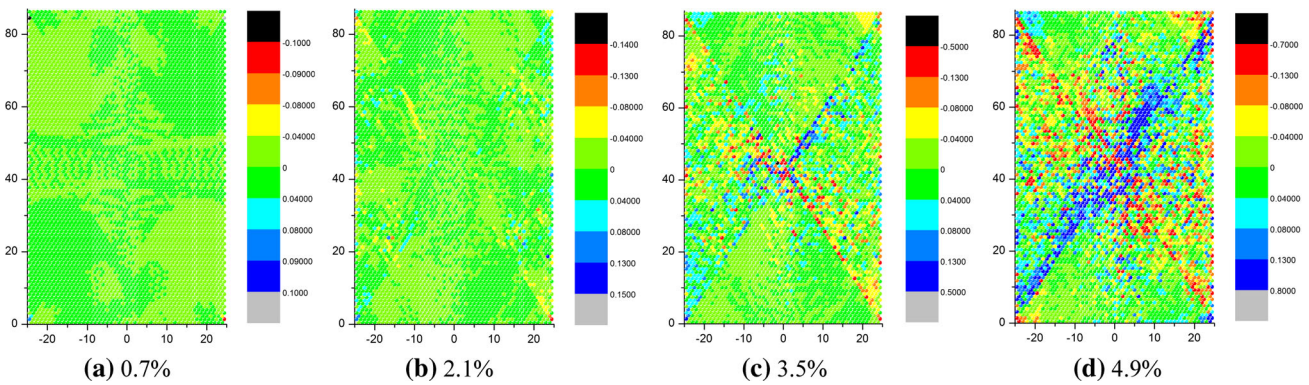

Fig. 9 The rotational angles distributions in the specimen with increasing axial strain in rolling resistance test 2

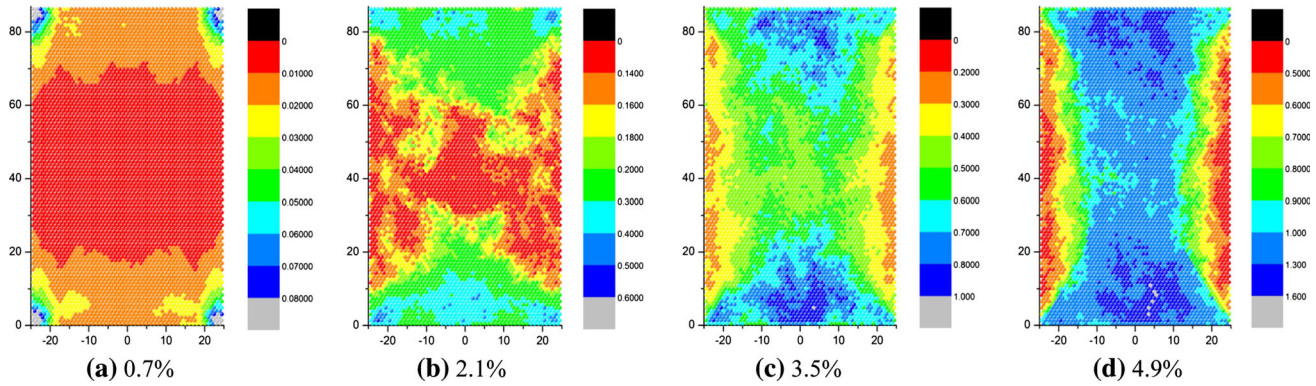

Fig. 10 The effective strain distributions in the specimen with increasing axial strain in no rolling test

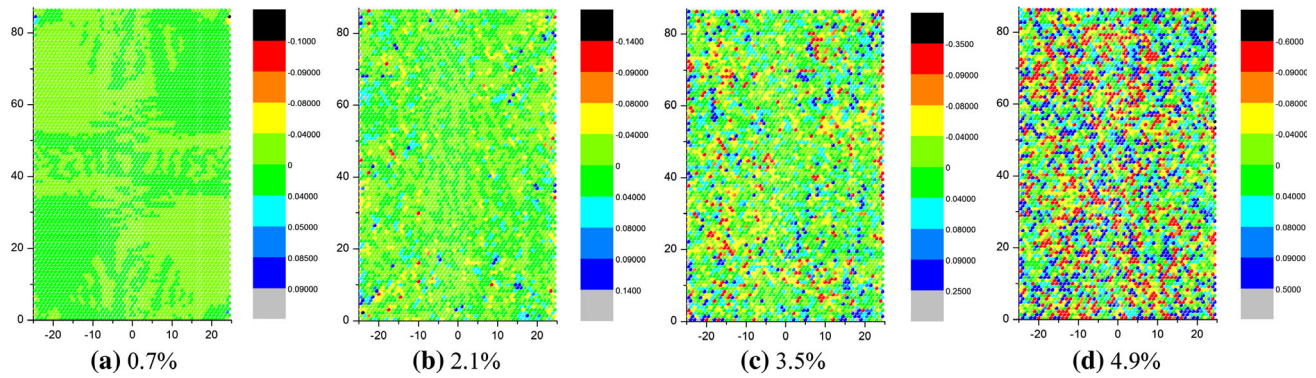

Fig. 11 The rotational angles distributions in the specimen with increasing axial strain in no rolling test

rotational bearings is the mechanism of reduction of strength and frictional dissipation in shear cells. Astrom et al. [11] also stated that the bearing state significantly reduces shear stiffness. These better explained why the strength is low when particle rolling takes place in previous conditions.

From Figs. 10 and 11, it can be observed that no shear bands can be seen in this condition, i.e. no rolling test. It also can be concluded that the development of distinct shear bands can be effectively simulated only when rolling resistance is considered in DEM.

4 Shear band failure of an imperfect specimen

An 86.7 cm × 50 cm particle assembly specimen is considered. To start, 4950 particles, each with an identical radius of 5 mm, are generated to form a specimen with an even porosity of 0.0931, and then some particles are replaced with particles with a porosity of 0.25. Rigid plates, on which the compression forces are applied, are set on the top and bottom of the specimen. Figure 12 shows the granular assembly of this specimen and the irregular arrangement in local areas. The boundary conditions and the material parameters incorporated in this analysis are identical to those used in the test of the perfect specimen.

4.1 Free rolling test

Figure 13 shows the deformation of the specimen and the position of the particles at different axial strains. It can be seen that some voids appear in the direction of imperfections. Figure 14 shows the effective strain distributions at different axial strains; the intense deformation initiates from imperfect areas and traverse the specimen gradually along the line connecting these two imperfect areas with the increasing axial strain in the specimen. Also, the shear band develops a little along another diagonal line in the specimen in later stage. The rotational angles of the particles, relative to the initial position, for different axial strains are shown in Fig. 15, which illustrates that high particle rotations appear in a wide conjugate diagonal range in the specimen at the end of loading stage, but the absolute value in the imperfect direction is larger. The deviatoric stress-axial strain curve for the free rolling test specimen, observed in Fig. 16, illustrates that the strength declines distinctly after the peak value and that the lowest value arrives at 6 % axial strain.

Compared with the numerical results (Figs. 4, 5, 6, 7) for the even specimen, the primary shear band initiates from the imperfect area and preferentially develops along the direction of imperfection in free rolling test. The width of the shear band is less than that of the previous one, while the effective

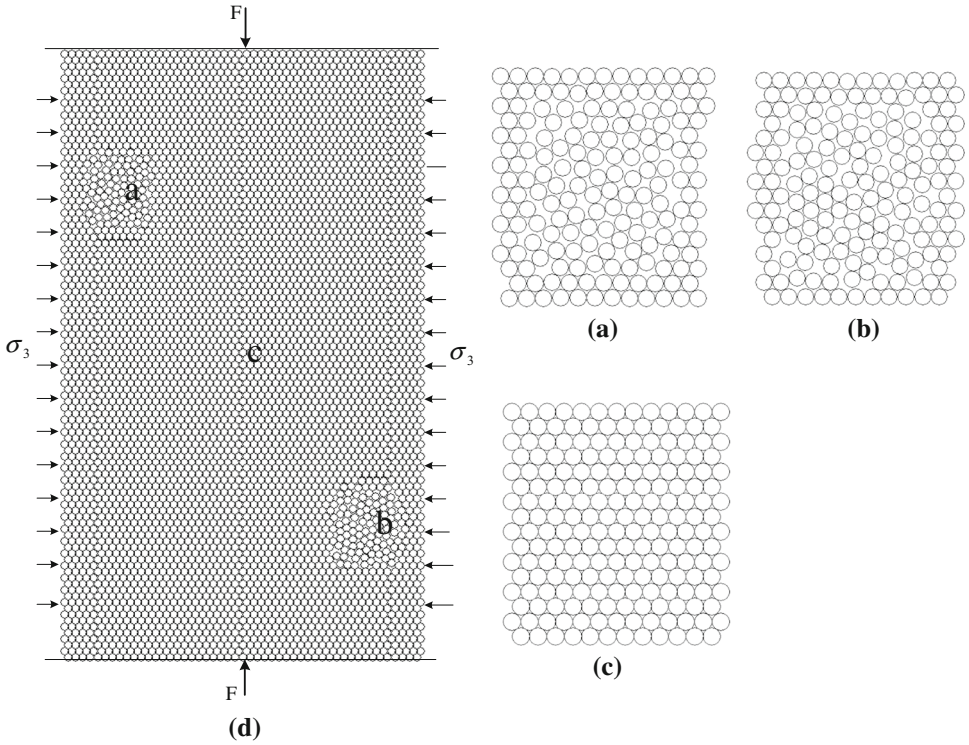

Fig. 12 A granular assembly by 4898 particles with radius of 5mm collocated in an irregular manner: **a**, **b** are irregular arrangement in local areas; **c** is regular arrangement; **d** is the whole specimen

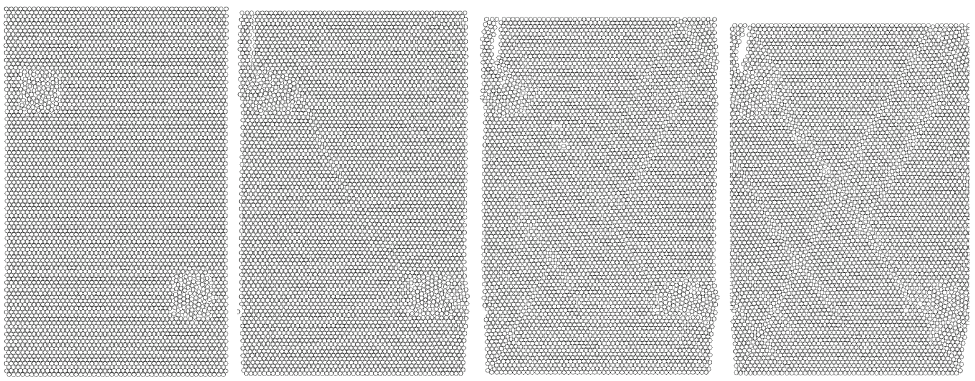

Fig. 13 The positions of the particles at different axial strains in the sample

strain and rotational angles of the particles in the shear band are greater. It means that the initial distribution of imperfections affects emergence and development of shear bands. The deviatoric stress-axial strain curve in Fig. 16 shows that the strength of the imperfect specimen is affected by the imperfections; it declines to 5.1 MPa less than 5.7 MPa of the even specimen.

4.2 Rolling resistance test 2

In this condition, the results are similar to the case of free rolling test. The intense deformation initiates from imperfect areas and distinct and regular shear bands develop gradually in the direction of imperfection with the increasing axial strain in the specimen. Also, a conjugate distinct shear band develops along another diagonal line in the specimen. The rotational angles of the particles illustrate that lower particle rotations in narrower zone compared with the free rolling test, and the development of minor shear bands is limited while the development of major shear bands is promoted in the rolling resistance test.

4.3 No rolling test

Figure 17 shows an almost uniform deformation of the specimen and the position of the particles at different axial strains. Figure 18 shows the effective strain distributions in the specimen at different axial strains, indicating that no regular shear bands are developed in the specimen. The rotational angles of the particles relative to the initial position, ran-

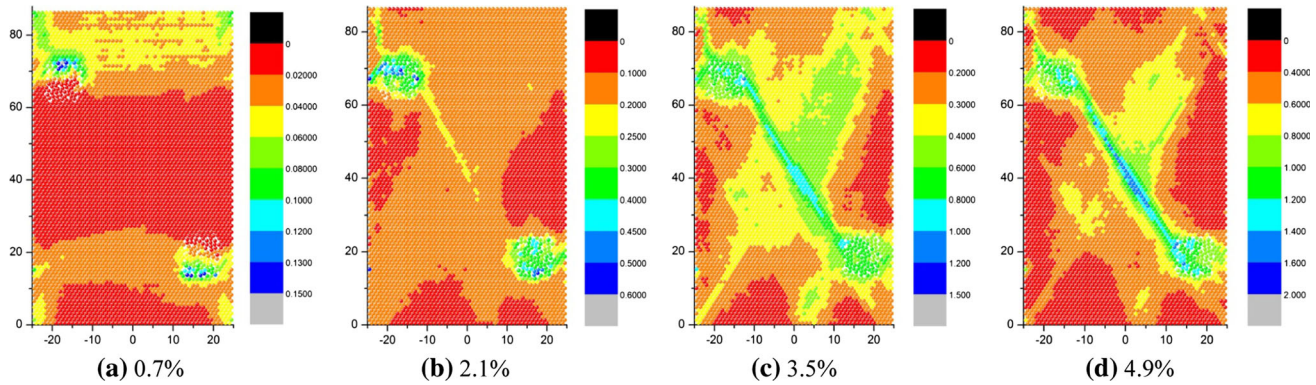

Fig. 14 The effective strain distributions in the granular assembly with increasing axial strain of the assembly in free rolling test

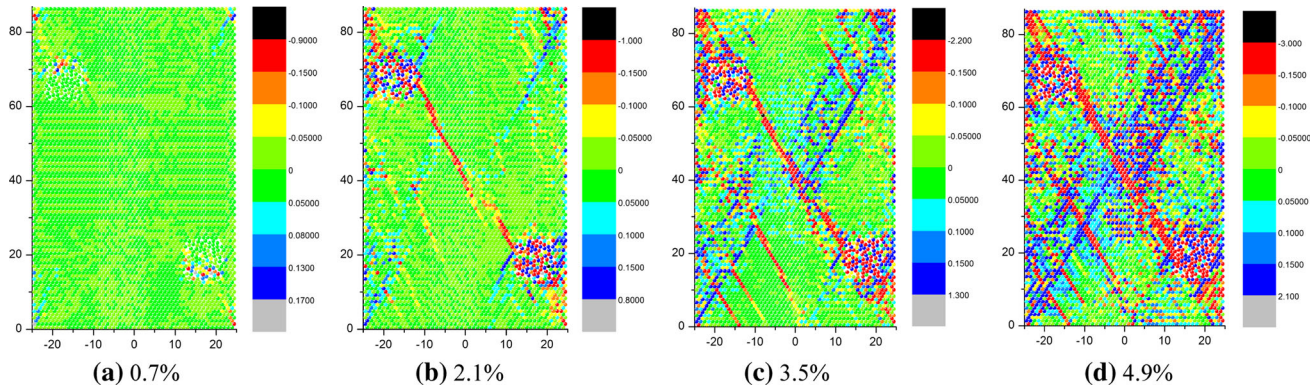

Fig. 15 The rotational angles distributions in the specimen with increasing axial strain in free rolling test

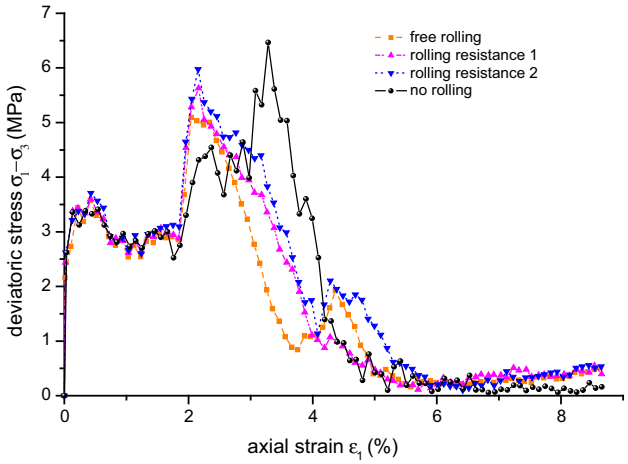

Fig. 16 The deviatoric stress-axial strain curve for the granular assembly

domly distribute in the specimen for different axial strains, as shown in Fig. 19. The deviatoric stress-axial strain curve for the no rolling test specimen, observed in Fig. 16, illustrates that a peak strength, which is the highest in these tests arrives at 3.5 % axial strain because the particles can not move smoothly. Therefore, the particle rolling influences not only the onset of shear band, but also the strength of the granular material.

Compared with the numerical results (Figs. 10, 11) for the even porosity distribution numerical simulation, there is still no clear shear band in this specimen, so it can be concluded that to well reproduce the development of distinct shear band in granular materials, it is very important to introduce rolling resistance into DEM. In addition, the strength of the specimen is affected by the imperfections; it declines to 6.5 MPa less than 7.6 MPa of the even specimen because the particles in imperfect areas can move more easily.

5 Conclusions

Particle rolling and imperfections are incorporated in the numerical model to study their influence on the formation of shear bands in granular materials. To describe the macroscopic deformation process and the emergence and evolution of shear bands in granular materials, the macroscopic definition of effective strain for granular materials is introduced. Several different numerical tests (i.e., free rolling test, rolling resistance test and no rolling test) using the discrete element method (DEM) are conducted to simulate the mechanical

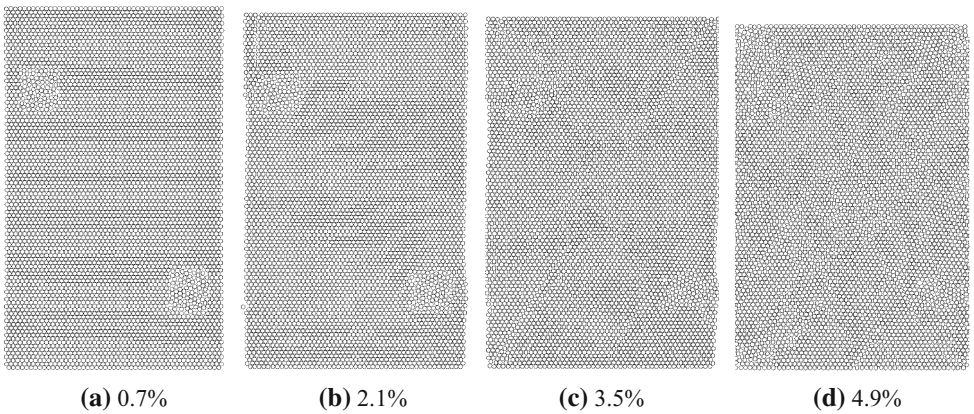

Fig. 17 The positions of the particles at different axial strains in the sample

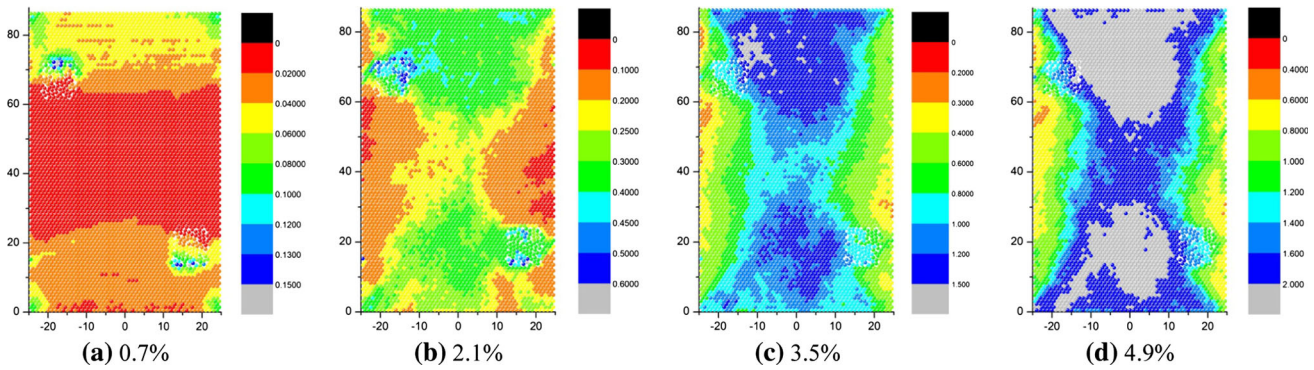

Fig. 18 The effective strain distributions in the granular assembly with increasing axial strain of the assembly in no rolling test

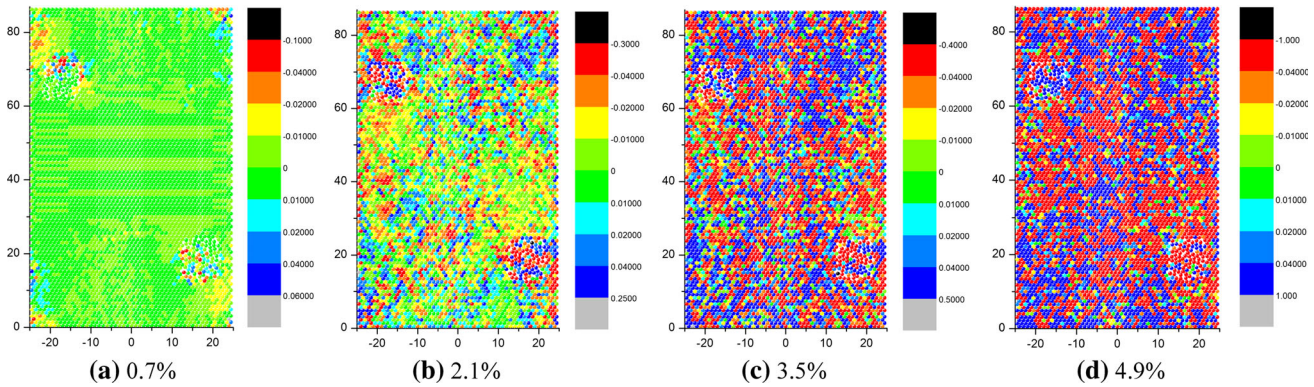

Fig. 19 The rotation distributions in the granular assembly with increasing axial strain of the assembly in no rolling test

response of the granular specimens. The deformed configuration, the progressive development of rotational angles and the distribution of effective strain in the granular specimens are illustrated to analyse the origination and evolution of shear bands. The following conclusions can be made:

1. The evolution of shear bands in granular materials is accompanied with particle rotation and void growth. The progressive development of rotational angles and effective strain both are capable of describing the emergence and evolution of shear bands in granular materials, but the latter is more effective.
2. The evolution of shear bands in granular materials can only be simulated effectively with particle free rolling and rolling resistance. In the case of particle rolling resistance, the shear band evolution is more distinct as the evolution of the minor shear bands is limited while the major shear bands are preferably promoted. It can be concluded that to well reproduce the development of distinct shear band in granular materials, it is very important to take into account rolling resistance in DEM.
3. The local rotating bearings play an important role in shear band formation. They influence both the onset of shear bands and the width of the shear bands, and decrease the

resistance and reduce the strength of the granular material. Usually speaking, the larger the rolling resistance is, the narrower the width of the shear band is.

4. The initial distribution of imperfections in the specimen affects the emergence and development of shear bands. Apparently, the primary shear bands initiate from the imperfect areas and develop preferentially along the direction of imperfections. As the rolling resistance increases, the conjugate shear bands, similar with that in even specimen, are developed in a late stage. Also, the strength of the imperfect specimen is lower than that of the even specimen. Therefore, the emergence and development of shear bands, which will result in a distinct decline in strength and eventually lead to instability and destruction of the material, can be effectively simulated when rolling resistance is incorporated in DEM and the initial distribution of imperfections in the granular material is defined.

Acknowledgments This work was financially supported by the National Natural Science Fund of China (11172216), the National Key Basic Research and Development Program (973 Program, 2010CB731502), and the Fundamental Research Funds for the Central Universities (DUT14LK20).

Appendix

The definition of effective strain for granular materials is briefly summarized.

To measure the change in position of a particle in relation to neighbouring particles, a nominal strain (i.e., the effective strain) is defined at the centre of the particle. Considering the change in position of particle A in relation to one of its neighbouring particles, denoted particle B and shown in Fig. 20, the nominal effective strain is defined as follows.

In Fig. 20, the relative change in position of two neighbouring particles at times t_1 and t_2 is considered. Using the XYZ global coordinate system, the centre coordinates of particles A and B are $\mathbf{X}_\mathrm{A}^1$,$\mathbf{X}_\mathrm{B}^1$ at t_1 and $\mathbf{X}_\mathrm{A}^2$, $\mathbf{X}_\mathrm{B}^2$ at t_2. The angles between the axis in the XYZ global coordinate system and the corresponding xyz local coordinate system are α_1, β_1, γ_1 at t_1 and α_2, β_2, γ_2 at t_2. The difference between the centre positions of particles A and B, using the global coordinate system, at t_1 and t_2 are

$$\Delta\mathbf{X}_{BA}^1 = \mathbf{X}_B^1 - \mathbf{X}_A^1; \quad \Delta\mathbf{X}_{BA}^2 = \mathbf{X}_B^2 - \mathbf{X}_A^2 \tag{2}$$

The differences based on the local coordinate system can be expressed as

$$\Delta\mathbf{x}_{BA}^1 = \mathbf{x}_B^1 - \mathbf{x}_A^1; \quad \Delta\mathbf{x}_{BA}^2 = \mathbf{x}_B^2 - \mathbf{x}_A^2 \tag{3}$$

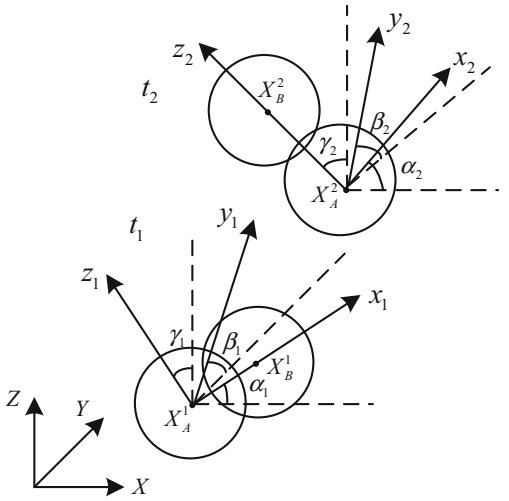

Fig. 20 The position of neighboring particles in different time

The coordinate transformation result is

$$\Delta\mathbf{x}_{BA}^1 = \mathbf{T}_1\Delta\mathbf{X}_{BA}^1; \quad \Delta\mathbf{x}_{BA}^2 = \mathbf{T}_2\Delta\mathbf{X}_{BA}^2 \tag{4}$$

where $\mathbf{T}_1$ and $\mathbf{T}_2$ are the coordinate transformation matrixes from the local coordinate system to the global coordinate system at t_1 and at t_2, respectively.

$$\mathbf{T}_1 = \begin{bmatrix} \cos\gamma_1 & \sin\gamma_1 & 0 \\ -\sin\gamma_1 & \cos\gamma_1 & 0 \\ 0 & 0 & 1 \end{bmatrix} \begin{bmatrix} \cos\beta_1 & 0 & -\sin\beta_1 \\ 0 & 1 & 0 \\ \sin\beta_1 & 0 & \cos\beta_1 \end{bmatrix} \tag{5}$$

$$\mathbf{T}_2 = \begin{bmatrix} \cos\gamma_2 & \sin\gamma_2 & 0 \\ -\sin\gamma_2 & \cos\gamma_2 & 0 \\ 0 & 0 & 1 \end{bmatrix} \begin{bmatrix} \cos\beta_2 & 0 & -\sin\beta_2 \\ 0 & 1 & 0 \\ \sin\beta_2 & 0 & \cos\beta_2 \end{bmatrix} \tag{6}$$

It means that by revolving β_1 around axis y_1, then γ_1 around axis z_1 at t_1, the local coordinate system can coincide with the global coordinate system. Similarly, by revolving β_2 around axis y_2, then γ_2 around axis z_2 at t_2, the local coordinate system can coincide with the global coordinate system.

As two-dimensional problem concerned, only the coordinate transformation within XY plane is considered [20]. The coordinate transformation matrixes are

$$\mathbf{T}_1 = \begin{bmatrix} \cos\alpha_1 & \sin\alpha_1 \\ -\sin\alpha_1 & \cos\alpha_1 \end{bmatrix}; \quad \mathbf{T}_2 = \begin{bmatrix} \cos\alpha_2 & \sin\alpha_2 \\ -\sin\alpha_2 & \cos\alpha_2 \end{bmatrix} \tag{7}$$

Deformation gradient f is used to describe the relative location change between particles A and B, from the material particle pair $A - B : \mathbf{X}_A^1 - \mathbf{X}_B^1$ at time t_1, to the same material particle pair $A' - B' : \mathbf{X}_A^2 - \mathbf{X}_B^2$ at time t_2, referred to as $x_1 - y_1$, where f is defined as:

$$f = \frac{\Delta \mathbf{x}_{\mathrm{BA}}^{2}}{\Delta \mathbf{x}_{\mathrm{BA}}^{1}} = \mathbf{RU} \tag{8}$$

In Eq. (8), **R** is the orthogonal tensor, which represents the rotation of the connecting line between particles A and B. **U** is a positive definite symmetric tensor, which represents the tensile deformation of the connecting line between particles A and B. They can be expressed as

$$\mathbf{R} = \begin{bmatrix} \cos(\alpha_2 - \alpha_1) & -\sin(\alpha_2 - \alpha_1) \\ \sin(\alpha_2 - \alpha_1) & \cos(\alpha_2 - \alpha_1) \end{bmatrix} \tag{9}$$

$$\mathbf{U} = \begin{bmatrix} \lambda_{\mathrm{AB}} & 0 \\ 0 & 1 \end{bmatrix} \tag{10}$$

$$\begin{cases} \lambda_{\mathrm{AB}} = \frac{l_{\mathrm{AB}}^{2}}{l_{\mathrm{AB}}^{1}} \\ l_{\mathrm{AB}}^{1} = \left\| \Delta \mathbf{x}_{\mathrm{BA}}^{1} \right\| \\ l_{\mathrm{AB}}^{2} = \left\| \Delta \mathbf{x}_{\mathrm{BA}}^{2} \right\| \end{cases} \tag{11}$$

Equations (4), (7), and (8) result in

$$\begin{cases} \Delta \mathbf{X}_{\mathrm{BA}}^{2} = \mathbf{F} \Delta \mathbf{X}_{\mathrm{BA}}^{1} \\ \mathbf{F} = \mathbf{T}_{2}^{\mathrm{T}} \mathbf{f} \mathbf{T}_{1} \end{cases} \tag{12}$$

According to the theory of continuum mechanics, the derivative tensor of the displacement gradient, defined by the relationship between the material coordinate and space coordinate, is

$$\mathbf{D} = \mathbf{F} - \mathbf{I} \tag{13}$$

where **I** is the unit matrix. If D_{ij} are the components of matrix **D**, then

$$\gamma_{\mathrm{AB}} = \left[\frac{2}{3} D_{ij} D_{ij} \right]^{1/2} \tag{14}$$

$$\gamma_{\mathrm{e}} = \frac{1}{n_A} \sum_{B=1}^{n_A} \gamma_{AB} \tag{15}$$

where γ_{AB} is an intermediate variable, and γ_{e} is the effective strain at the centre of particle A, around which there are n_{A} neighbouring particles.

References

1. Cundall, P.A., Strack, O.D.L.: A discrete numerical model for granular assemblies. Geotech **29**, 47–65 (1979)
2. Chang, C.S., Misra, A.: Packing structure and mechanical properties of granulates. J. Eng. Mech. **116**, 1077–1093 (1988)
3. Zhang, D., White, W.J.: An efficient calculation method for particle motion in discrete element simulations. Powder Technol. **98**, 223–230 (1998)
4. Oda, M., Iwashita, K.: Mechanics of Granular Materials. Ballkema, Rotterdam (1999)
5. Al-Raoush, R.: Microstructure characterization of granular materials. Phys. A **377**, 545–558 (2007)
6. Hare, C.L., Ghadiri, M.: Influence of measurement cell size on predicted attrition by the Distinct Element Method. Powder Technol. **236**, 100–106 (2013)
7. Oda, M., Konishi, J., Nemat-Nasser, S.: Experimental micromechanical evaluation of strength of granular materials: effects of particular rolling. Mech. Mater. **1**, 269–283 (1982)
8. Oda, M., Takemura, T., Takahashi, M.: Microstructure in shear band observed by microfocus X-ray computed tomography. Geotechnique **54**, 539–542 (2004)
9. Bardet, J.P.: Observations on the effects of particle rotations on the failure of idealized granular materials. Mech. Mater. **18**, 159–182 (1994)
10. Veje, C.T., Howell, D.W., Behringer, R.P.: Kinematics of a two-dimensional granular Couette experiment at the transition to shearing. Phys. Rev. E **59**, 739–745 (1999)
11. Åström, J.A., Herrmann, H.J., Timonen, J.: Granular packings and fault zones. Phys. Rev. Lett. **84**, 638–641 (2000)
12. Alonso-Marroquín, F., Vardoulakis, I., Herrmann, H.J.: Effect of rolling on dissipation in fault gouges. Phys. Rev. E **74**, 031306-1–031306-10 (2006)
13. Iwashita, K., Oda, M.: Rolling resistance at contacts in simulation of shear band development by DEM. J. Eng. Mech. **3**, 285–292 (1998)
14. Oda, M., Kazama, H.: Microstructure of shear bands and its relation to the mechanisms of dilatancy and failure of dense granular soils. Geotechnique **48**, 465–481 (1998)
15. Iwashita, K., Oda, M.: Micro-deformation mechanism of shear banding process based on modified distinct element method. Powder Technol. **109**, 192–205 (2000)
16. Tordesillas, A., Stuart Walsh, D.C.: Incorporating rolling resistance and contact anisotropy in micromechanical models of granular media. Powder Technol. **124**, 106–111 (2002)
17. Jiang, M.J., Yu, H.S., Harris, D.: A novel discrete model for granular material incorporating rolling resistance. Comput. Geotech. **32**, 340–357 (2005)
18. Mohamed, A., Gutierrrez, M.: Comprehensive study of the effects of rolling resistance on the stress-strain and strain localization behavior of granular materials. Granul. Matter **12**, 527–541 (2010)
19. Feng, Y.T., Han, K., Owen, D.R.J.: Some computational issues numerical simulation of particulate systems. In: Fifth World Congress on Computational Mechanics, Vienna, Austira (2002)
20. Li, X.K., Chu, X.H., Feng, Y.T.: A discrete particle model and numerical modeling of the failure modes of granular materials. Eng. Comput. **22**, 894–920 (2005)
21. Tejchman, J.: Effect of fluctuation of current void ratio on the shear zone formation in granular bodies within micro-polar hypoplasticity. Comput. Geotech. **33**, 29–46 (2006)
22. Borja, R.I., Song, X.Y., Rechenmacher, A.L., Abedi, S., Wu, W.: Shear band in sand with spatially varying density. J. Mech. Phys. Solids **61**, 219–234 (2013)
23. Herrmann, H.J.: Granular matter. Phys. A **313**, 188–210 (2002)
24. Vardoulakis, I., Graf, B.: Shear band formation in fine-grained sand. In: Proceeding of Fifth International Conference Numerical Methods in Geomechanics, Nagoya, Balkema, Rotterdam (1985)
25. Oda, M., Iwashita, K.: Study on couple stress and sear band development in granular media based on numerical simulation analyses. Int. J. Eng. Sci. **38**, 1713–1740 (2000)
26. Chu, X.H.: The discrete particle and coupled discrete-continuum models and numerical methods for granular materials. PhD dissertation, DLUT, Dalian (2006)